Influence of machining damage generated during trimming of CFRP composite on the compressive strength

N Nguyen-Dinh, Christophe Bouvet, Redouane Zitoune

Influence of machining damage generated during trimming of CFRP composite on the compressive strength

N Nguyen-Dinh[1,2], C Bouvet[1] and R Zitoune[1]

Abstract

Machining of composite materials is a challenging task due to the heterogeneity and anisotropy of composite structures. The induced defects reduce integrity of the machined surface as well as the loading capacity of the composite structure in service. Therefore, it is necessary to quantify the damage induced during trimming and correlate the quality of the machined surface to mechanical properties. The correlation of the surface roughness criteria, widely used in literature, to the mechanical behavior raise several contradictions. For this reason, new parameters for the characterization of the machined surface are proposed and correlated to the mechanical behavior under compressive loading. In this context, carbon fiber-reinforced plastic laminates are conventionally trimmed, and the machining damage is characterized using scanning electron microscope observations, X-ray tomography, and 3D optical topography. The results reveal that crater volume and maximum depth of damage quantify the machining damage more realistic compared to the classical surface roughness criteria.

Keywords

Composite materials, machining, mechanical testing, surface analysis

Introduction

Fiber-reinforced plastic (FRP) composites own several advantages when compared to metallic materials, e.g. a very high strength-to-weight ratio, a high modulus-to-weight ratio, and a good corrosion resistance. For this reason, FRP composites have been used in many important fields like aerospace, robotics, shipping, sport equipment, and defense applications. In industry, composite parts are usually fabricated to near net shape. However, after demolding, to obtain the required geometrical tolerances necessary for assembly, some machining operations are always essential such as: drilling, milling/trimming, grinding, and turning in both conventional processes[1–3] and nonconventional processes.[4,5]

As known, composite materials are typically composed of minimum two different materials, i.e. fiber for reinforcement and matrix. However, these materials have different mechanical, thermal, and physical properties which make composite materials inhomogeneous and anisotropic. These properties lead to difficulties during machining using conventional process compared to isotropic materials. In fact, the mechanisms of chip formation process in composite materials are accompanied by several damages located on the machined surface and also the free edges of the specimens.[6–10] In fact, during the trimming operation the defects appearing along the free edge of machined surface are delamination, cracks uncut fibers,[11–14] while defects occurring on the machined surface are fiber pullout, matrix cracking, and thermal/mechanical matrix degradation.[3,15–19] It is clear that the occurrence of machining damage creates many stress concentration zones which may influence the mechanical behavior of the machined composite structures.

Sheikh-Ahmad and Shahid[14] have conducted the edge trimming of carbon fiber-reinforced plastic

[1]Institut Clément Ader, Université de Toulouse, France
[2]Faculty of Mechanical Engineering, Thai Nguyen University of Technology, Vietnam

Corresponding author:
C Bouvet, Institut Clément Ader 3, rue Caroline Aigle Toulouse 31400, France.
Email: christophe.bouvet@isae.fr

(CFRP) laminates to determine the influences of cutting parameters on the machining quality which is characterized by surface roughness (R_a, R_z) and mode I delamination. The result shows that depth of mode I delamination increases with an increase in feed speed and a decrease in cutting speed (i.e. increase in theoretical chip thickness). The occurrence of mode I delamination is due to the application of axial cutting force component on outer layer. This was confirmed by the study of Prakash et al.[16] in which CFRP laminates were trimmed using three tool geometries made of tungsten carbide, namely burr tool with tool shape of trapezoidal (T1), burr tool with tool shape of pyramidal (T2) and four fluted helical end mill (T3). It was observed that tools T1 and T2, which produce smaller axial cutting force component, generate minimum depth of delamination, while maximum depth of delamination was seen in free edge of composite part machined by tool T3 which produces highest axial cutting force component when compared to those resulting from tools T1 and T2. In addition to tool geometry, cutting parameters and tool wear have also strong influence on the generation of delamination.[20–21] When trimming CFRP laminates using polycrystalline diamond (PCD) tool, Wang et al.[20] observe that delamination increases with increasing in feed speed and decreasing in cutting speed. This is because increase in feed speed and a decrease in cutting speed result the augmentation of chip thickness which requires higher level of cutting forces. Finally, higher level of cutting forces will cause higher level of delamination. In another study, Hintze et al.[12] and Wang et al.[21] state that the increase of cutting edge radius of tool is also a crucial factor affecting on the generation of delamination where no delamination is observed when machining is performed using a sharp tool. It is important to mention that the defects occurring along the free edge of machined surface is considered as critical damage which can seriously impact the endurance limit.[22]

Concerning the machining damage located on the machined surface, the relative angle between fiber direction and cutting direction is one of the main factors affecting the chip formation.[7–10] This is because of difference in cutting mechanism. Additionally, cutting parameters (cutting speed, feed speed, and depth of cut), tool wear, and tool materials also have significant influence. To quantify these kinds of damage, roughness criterion has been used so far. Many studies have shown that an increase in feed speed and a decrease in cutting speed typically cause a higher level of machining damage.[3,13,14,23,24] Slamani et al.,[3] when CFRP laminates were trimmed using CVD tool with six straight flutes, have shown that the combination of high cutting speed and low feed rate induces low level of damage. This is due to the fact that an increase in cutting speed and a decrease in feed speed generate minimum theoretical chip thickness which makes ease of machining. Similar phenomena were also observed in the studies of Sheikh-Ahmad et al.[13] and Janardhan et al.[25] Recently, Nguyen-Dinh et al.[26] have revealed reverse results in which the combination of high cutting speed (250 m/min) and low feed speed (500 mm/min) generates severe damage in the machined surface. The difference of results between studies was explained by the authors. Indeed, when the feed speed decreases, the time of contact between the CFRP specimen and cutting tool increases. However, due to the abrasive character of the carbon fibers, the frictional phenomenon at the interface (CFRP/tool) intensifies leading to the augmentation of the machining temperature. This leads to acceleration of the tool wear; hence, poor quality of the machined surface is obtained under the action of blunt cutting edge. Similar results have been shown during dry drilling of 3D woven composite by Cadorin et al.[27] If we refer to the literature, the machined surface quality is characterized by the surface roughness criteria (R_a or S_a) and then correlated to the mechanical behavior of composite structures.[14,28–31] However, the use of surface roughness criteria to quantify the machining damage in composite materials is not convincing. Indeed, when carrying out the compression test of unidirectional composite, Squires et al.[31] have documented that an increase in surface roughness (R_a) leads to reduction in the compressive strength. In the work of Sheikh-Ahmad and Shahid,[14] similar relation between tensile strength and surface roughness (R_z), i.e. an increase in surface roughness causes a reduction of tensile strength is found. Based on these results, it seems that the surface roughness (R_a) is a good indicator to characterize the machined surface of composite materials. However, in other research work, contradictory results have been observed. For example, Arola and Ramula[28] have conducted bending tests of carbon/epoxy composite laminates which were machined by three methods, i.e. abrasive water jet (AWJ), circular diamond saw (DS), and conventional trimming by PCD tool. The results showed that specimens machined by DS are characterized by lowest value of R_a, while specimens machined by PCD exhibit highest value of R_a. However, the authors realize that the Weibull modulus and average strength of the trimmed specimens are almost similar. Based on this result, they conclude that surface quality has no influence on flexural properties or in other words R_a is not enough to quantify the machining damage generated during machining composite materials. In case of testing unidirectional glass/epoxy composite (45°) under tensile loading, Ghidossi et al.[29] have revealed that tensile strength increases with the increasing of the surface roughness (R_a). In addition, Haddad et al.[32] have conducted the

compression test of machined specimens under three different classifications. This classification was based on the temperature generated during machining, viz. inferior to 130°C (group one), between 130°C and the glass transition temperature of the matrix used which is $T_g = 187$°C (group two) and superior to the T_g of the matrix (group three). The obtained results reveal that tested specimens in the first group exhibit highest compressive strength, while the specimens in the third group have lowest compressive strength. Totally, compressive strength of specimens reduces 29% for the group three compared to the group one. Apart from the difference in the machining temperature, the surface roughness of the group one and three varies from 4 µm to 29 µm, respectively. However, within each group of specimens (particularly for the group one and group two), it was observed that surface roughness has no clear significant influence on compressive strength. Thus, it can be said that surface roughness is not a representative indicator to quantify the machined surface and to correlate to the mechanical behaviors of composite parts. Sheikh-Ahmad et al.,[13] Arola and Ramula,[28] Ghidossi et al.,[29] Ramulu[33] believe that internal damage (cracks) under the machined surface or subsurface damage which cannot be detected by stylus, underestimates the machining quality leading to wrong prediction of the failure stress of composite parts. To overcome this issue Ghidossi et al.[29] have proposed two new parameters, namely "percentage of damaged surface" and "depth of subsurface cracking", to quantify the damage under machined surface when trimming of unidirectional specimens oriented at +15° and ±45 compared to the direction of loading (tensile). The results revealed that a reduction of ultimate stress was seen when "percentage of damaged surface" increases, while an increase in "depth of subsurface cracking" leads to decrease ultimate stress. However, the correlation of these new parameters is not clear in the case of specimens oriented at –45°. Recently, when performing the milling of multidirectional CFRP laminates by AWJ process for composite repair application, Hejjaji et al.[5] have quantified machining damage by measuring volume of total craters generated in the machined surface. Total crater volume (C_v) was correlated to tensile strength and endurance limit during fatigue loading on unidirectional and multidirectional specimens. The obtained results have shown clearly that the C_v criterion is more representative of the machining quality compared to the surface roughness criteria (S_a and R_a).

The objective of this paper is to evaluate the effect of machining damage (after trimming), which is characterized using crater volume and internal depth of damage, on the compression strength and on the failure scenario observed during compression test. To generate various levels of surface quality (different forms and size of damage), the machining parameters have been purposely selected. In addition, the machined surfaces are characterized at micro (surface texture) and macro (damage size) scales using 3D optical topography and scanning electron microscopy (SEM). The X-ray tomography technique is also utilized to measure the internal depth of damage under the machined surface. The characterization of machining damage is also performed using the surface roughness criterion (R_a). Moreover, new parameters, named crater volume (C_v) and maximum depth of damage (D), are proposed and correlated to the mechanical properties. After the surface characterization and during the compression test, the machined specimens are multi-instrumented by extensometer for the strain measurement, and an infrared camera is used to evaluate the damage scenario.

Experimental procedure

Material preparation

The CFRP laminates used in this study were made of unidirectional Prepregs supplied by Hexcel Composite Company and referenced under HEXPLY T700 268 M21 34% (T700-M21). Twenty layers of prepregs corresponding to the dimension of 300 mm × 300 mm and a thickness of 0.26 mm were stacked together to create plates with a theoretical thickness of 5.2 mm with the following layup with respect to feed direction: $[90_2/–45/0/45/90/–45/90/45/90]_S$. These plates were compacted during 12 h using a vacuum pump in a controlled atmosphere (white room). A mold for the laminate was prepared and placed in a vacuum bagging and evacuated to 0.7 bar (as recommended by Hexcel Composite Company, Figure 1). Curing was then carried out at 180°C for 120 min during which the pressure was maintained at

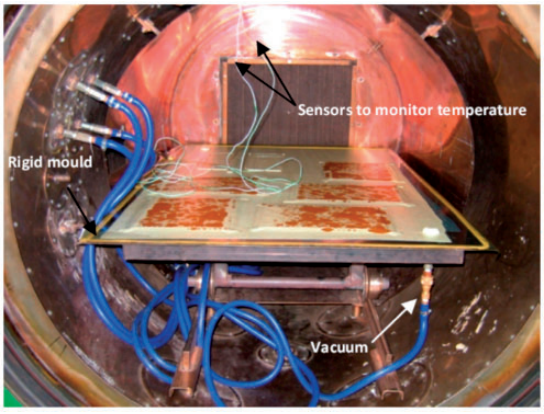

Figure 1. Composite laminates after the curing process in the autoclave.

Table 1. Mechanical properties of HexPly T700-M21.

Composite materials (T700/M21)	Ply thickness: 0.26 mm Fiber content: $V_{fiber} = 59\%$ Stacking sequence with respect to the feed direction for group A: $[90_2/-45/0/45/90/-45/90/45/90]_S$ Stacking sequence with respect to the feed direction for group B:$[0_2/45/90/-45/0/45/0/-45/0]_S$ Young modulus: $E_l = 142$ GPa, $E_t = 8.4$ GPa Shear modulus: $G_{lt} = 3.8$ GPa Glass transition temperature: $T_g = 187°C$ Energy release rate: $G_{IC} = 0.35$ N/mm, $G_{IIC} = 1.21$ N/mm Young modulus in X direction of group A: $E_x = 32.9$ GPa Young modulus in X direction of group B: $E_x = 82.6$ GPa

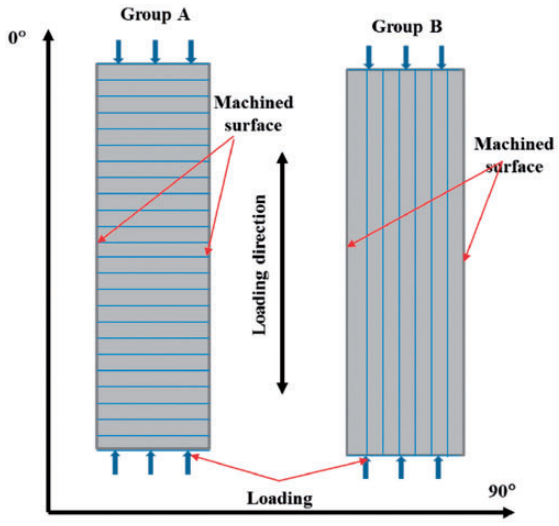

Figure 2. Schema of loading direction during compression test in group A and group B specimens.

7 bars in an autoclave. The temperature rise rate in the autoclave was 5°C/min. The mechanical properties of the ply T700-M21 are detailed in Zitoune et al.[34] This stacking sequence is used in the structural part of the A350 aircraft of Airbus.[32,35] To reduce the variability of the mechanical properties due to the process of manufacturing, all the specimens used in this study are cured together in the same mold. The mechanical properties of composite materials are presented in the Table 1.

Specimen preparations

A full factorial design of cutting condition, including three levels of feed speeds and two levels of cutting speeds, was studied. To generate different level of mechanical degradations an extreme condition combining the highest cutting speed (339 m/min) and the lowest feed rate (29 mm/min) was selected. These were the highest cutting speed value and the lowest feed speed value available in the used machine tool. A radial depth of cut of 2 mm is used for all the specimens of machining test. In fact, for these reasons the cutting conditions and the machining configuration (down milling) were chosen to generate different levels of mechanical degradations.

It can be noticed that specimens were prepared according to the standard recommendation AFNOR NF T 51-120-3 (1995). Tested specimens were prepared in two groups, named group A and group B. Group A includes the specimens with dominant 90° layers, while group B includes the specimens with dominant 0° layers. The interest of this choice is to highlight the influence of fiber and matrix damage on the compression failure. Indeed, the machining induces more matrix damage than fiber damage, and therefore, the group A, which is matrix dominated, should be more affected by machining damage than group B, which is fiber dominated. The schematic figuration of tested specimens of group A and group B can be seen in Figure 2. A pre-cut was carried by AWJ process. By this way, the recommended dimensions of each specimen before trimming are 280 mm × 14 mm × 5.2 mm. For each machining condition and for each tool, three specimens were machined by using a new PCD cutter with two straight flutes (Figure 3). The machining is conducted without lubricant (dry machining). The detail information of experimental parameters is presented in Table 2.

Characterization of the machined surface

The machining quality has been investigated by three different techniques. The first technique concerns the 3D topographer "Altisurf 520" which works based on the principle of a non-contact stylus (Figure 4). The evaluation area of 8 mm × 4.5 mm (corresponding to direction of length and thickness, respectively) was scanned with a spatial resolution of 4 μm. 3D average surface roughness were extracted from the topography using "Digitalsurf" software using Gaussian filter (cut-off = 0.8 mm). Moreover, craters occurring on the machined surface were estimated by their volume by analyzing the topography surface using the software Mountain maps. The volume calculation is performed based on the polynomial (with degree 3) approximation technique. The second technique of the surface characterization is based on the use of the SEM. For this, the SEM used is referenced under "JEOL-JSM 5310". Finally, to quantify the internal damage of the machined specimens, the X-ray tomography was

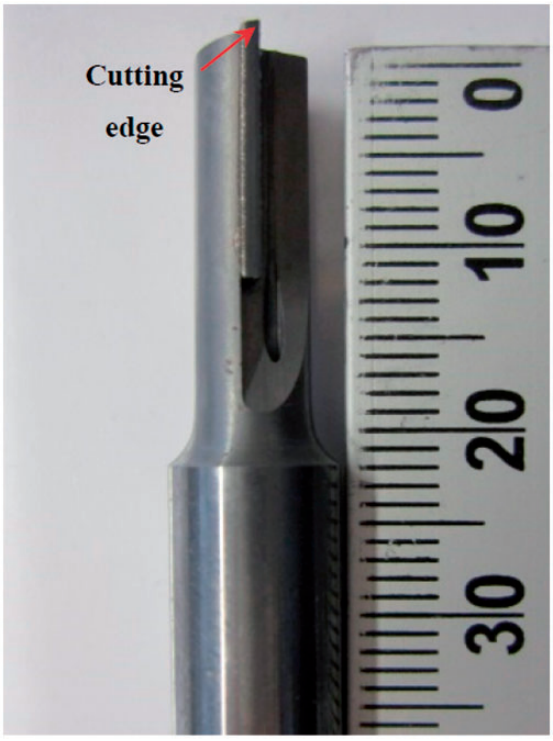

Figure 3. PCD tool used with two straight flutes.

Table 2. Summary of experimental conditions for trimming of CFRP laminates.

Cutting tools	PCD tool: helix angle = 0°, rake angle = 5°, clearance angle = 7° Diameter = 6 mm Number of cutting edge = 2
Cutting conditions	Radial depth of cut (a_e) = 2 mm Full factorial design Feed rate (mm/min): V_f = 500, 1000, and 1500 Cutting speed (m/min): V_c = 150 and 250 Extreme condition Feed rate (mm/min): V_f = 29 Cutting speed (m/min): V_c = 339

CFRP: carbon fiber-reinforced plastic; PCD: polycrystalline diamond.

conducted using Micro-Tomography Easy Tom 130 machine (Figure 5). The detailed descriptions of previous measurements can be found in Nguyen-Dinh et al.[26]

Quasi-static compression tests

After machining test, machining damage was characterized as previously mentioned. Fifteen specimens of group A and 12 specimens of group B (total 27

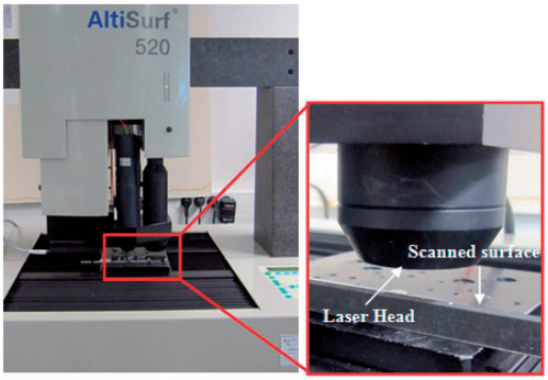

Figure 4. Confocal microscope for 3D topography measurement.

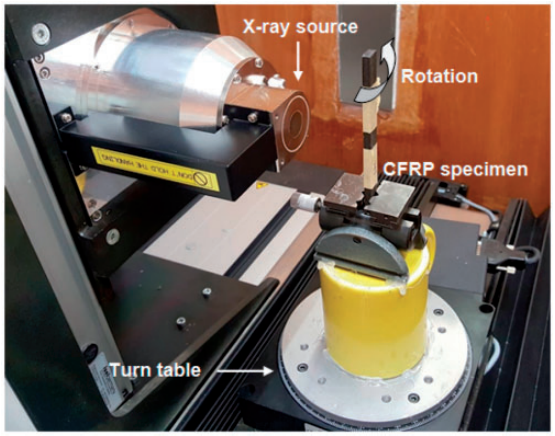

Figure 5. X-ray tomography for specimens analyzing.

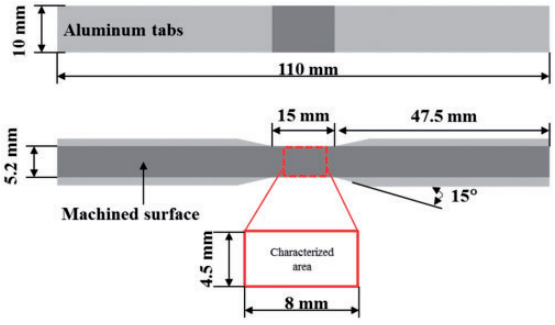

Figure 6. Schematic shape of the specimens according to AFNOR NF T 51-120-3 standard.

specimens) were tabbed following the AFNOR NF T 51-120-3 standard (Figure 6).

To study the influences of machining damage on mechanical behaviour, specimens with different levels of machining quality (good, medium, and poor surface quality) were purposely selected from specimens trimmed with cutting conditions mentioned in

Table 2. The items are named of good, medium, and poor surface quality based on the value of surface roughness and crater volume. Compression test was performed on an Instron testing machine. Specimens were prepared according to AFNOR NF T 51-120-3. To eliminate dynamic effect, displacement control loading was setup by 0.5 mm/min. During the compressive loading, specimens were instrumented using an extensometer, meanwhile failure process can be observed using an infrared camera. The details of experimental devices used during compression test are shown in the Figure 7.

Results and discussion

Machined surface and damage

To visualize damage appearing in the machined surface of specimens which are selected for compression test (15 specimens and 12 specimens for group A and B, respectively), SEM observations have been carried out. Figure 8 presents the SEM images of specimens in group A machined at various cutting distances (L_c). It can be seen that in case of good machining quality, it is difficult to distinguish the machined damage induced in the different layer orientations of

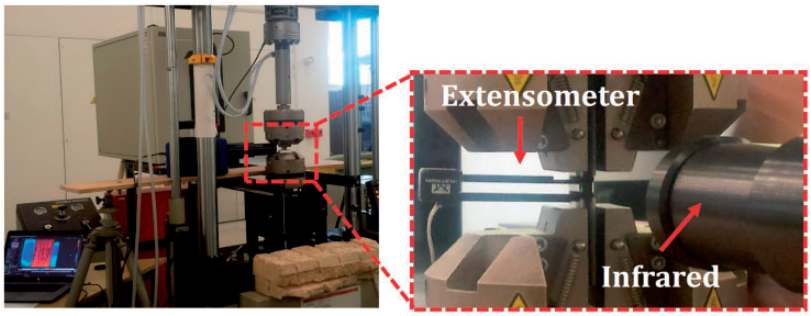

Figure 7. Experimental devices for compression tests.

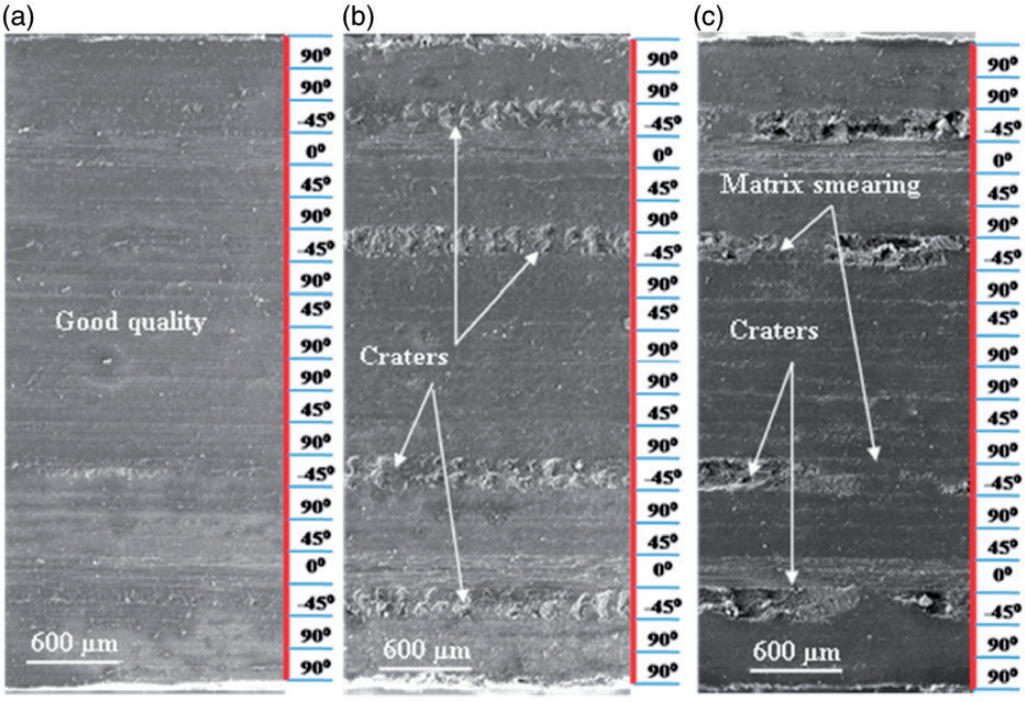

Figure 8. SEM images of machined surface for specimens of group A (a) good quality with $V_c = 150$ m/min, $V_f = 500$ mm/min, and $L_c = 0.28$ m, (b) medium quality with $V_c = 150$ m/min, $V_f = 1500$ mm/min, and $L_c = 1.68$ m, and (c) poor quality with $V_c = 339$ m/min, $V_f = 29$ mm/min, and $L_c = 0.28$ m.

stacking sequence. However, in case of specimens with medium and poor surface quality, we observe that different kinds of defects in forms of craters, fiber pullout, and matrix smearing are visualized on the trimmed surfaces. These defects, however, are located in the –45° layers (or 45° depending on the relative position between feed direction and fiber orientation). The difference between the levels of machining damage is strongly impacted by cutting parameters (cutting speed and feed speed) and the status of cutting tool (tool wear). The influences of these factors on the machining damage induced have been detailed in Nguyen-Dinh et al.[26] Similarly, the different levels of machining damage are also visualized in the machined surface of specimens in group B (Figure 9) where defects in forms of craters or holes are mainly observed in the –45° layer fibers. Logically, the areas and depth of craters across machined surface with poor quality specimens seem more important than those with medium quality.

Due to the incompetence of roughness criterion as mentioned earlier, it is necessary to suggest new parameters which better quantify machining damage to mechanical behaviors. Topographies are performed to provide the dimensional information of damage features. Topography profiles showing dimensional information of damage of specimens in group A and group B are presented in Figures 10 and 11, respectively. Craters are dominantly observed, and their depth, area, and volume of crater vary with cutting parameters.[26] In this context, craters are estimated by their volume to quantify machining damage. It can be seen that the maximum depth of craters in the machined surface of specimen with good quality is around 15 μm. Nevertheless, this value increases 4 and 8 times in case of specimens with medium quality and poor quality, corresponding to 60 μm and 120 μm, respectively (Figure 10). Similarly, in case of group B specimens, the maximum depth of craters occurring in machined surface of specimens with good quality, medium quality, and poor quality approximately estimated by confocal technique are 20 μm, 70 μm, and 110 μm, respectively (Figure 11). Based on these results, it can be said that topography profiles of specimens correctly reflect the damage forms which is demonstrated by SEM images. The total crater volumes in measured areas of tested specimens will be correlated to compressive strength in the last section of this paper.

As previously presented, SEM results provide the strong description of damage appearing in the machined surface. However, we can see that matrix smearing appears in some places in the machined surface. Hence, it is difficult to precisely know the shapes and depth of damage inside the machined surface. By this reason, X-ray tomography was performed. The protocol of getting X-ray tomography images was

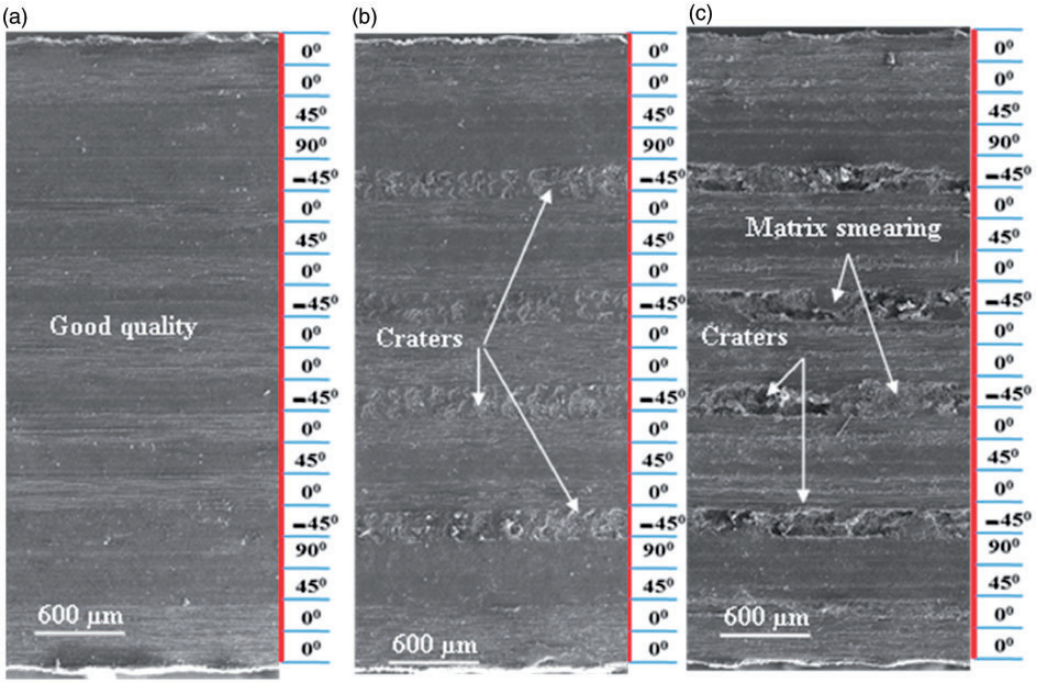

Figure 9. SEM images of machined surface for specimens of group B (a) good quality with $V_c = 150$ m/min, $V_f = 500$ mm/min, and $L_c = 0.28$ m, (b) medium quality with $V_c = 150$ m/min, $V_f = 1500$ mm/min, and $L_c = 1.68$ m, and (c) poor quality with $V_c = 339$ m/min, $V_f = 29$ mm/min, and $L_c = 0.28$ m.

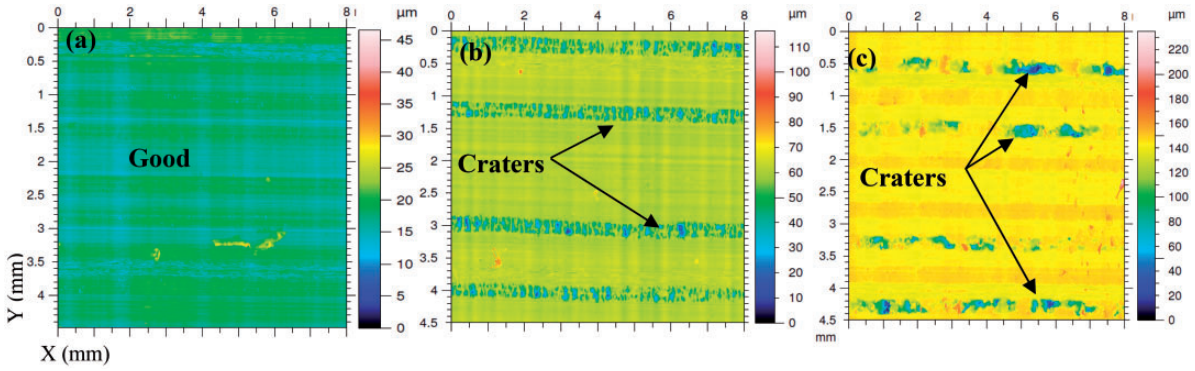

Figure 10. Topography profiles showing the appearances of craters on the machined surface for the group A (a) good quality with $V_c = 150$ m/min, $V_f = 500$ mm/min, and $L_c = 0.28$ m, (b) medium quality with $V_c = 150$ m/min, $V_f = 1500$ mm/min, and $L_c = 1.68$ m, and (c) poor quality with $V_c = 339$ m/min, $V_f = 29$ mm/min, and $L_c = 0.28$ m.

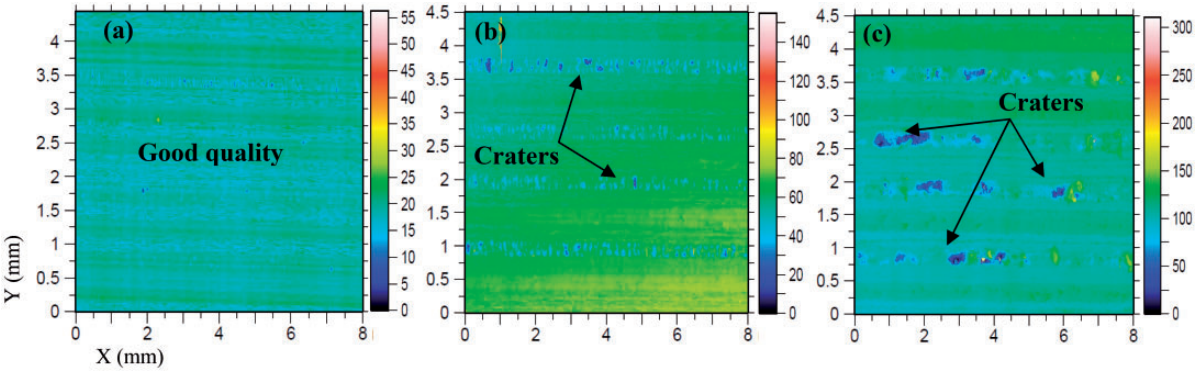

Figure 11. Topography profiles showing the appearances of craters on the machined surface for the group B (a) good quality with $V_c = 150$ m/min, $V_f = 500$ mm/min, and $L_c = 0.28$ m, (b) medium quality with $V_c = 150$ m/min, $V_f = 1500$ mm/min, and $L_c = 1.68$ m, and (c) poor quality with $V_c = 339$ m/min, $V_f = 29$ mm/min, and $L_c = 0.28$ m.

detailed in Nguyen-Dinh et al.[26] Figures 12 and 13 present the machining damage occurring under machined surface of group A and group B specimens, respectively. It can be seen that at the similar 30 μm depth of scanning (DoS), defects generated during machining are not visualized in case of specimen with good quality. Nevertheless, in case of specimens with medium quality, the damage in the form of craters is observed mainly at the –45° layer positions of machined surfaces (Figure 12(b)). In particular, the level of damage, both frequency and altitude, increases in case of poor quality specimens (Figure 12(c)). The evolution of damage formed under machined surface also similarly varies from specimens with good quality to specimens with poor quality in case of group B. X-ray tomography images one more time confirm insistently the machining damage which is shown in Figures 8 and 10 for group A (Figures 9 and 11 for group B). The appearances of craters in machined surface can highly impact on the loading ability of composite specimens. The relationships between machining damage characterized using crater volume, maximum depth of damage (D) given by X-ray tomography (representative by DoS), and compression behavior will be discussed in the next section of this study.

Compression test

Specimens in group A (15 specimens) and group B (12 specimens), which are characterized for machining damage as previously presented, are subjected to compressive loading. It is noticed that representative values of crater volume (C_v), as well as maximum depth of damage (D), are obtained by averaging their values in both sides of machined surface of each tested specimen. The schema of compression test can be seen in Figure 14.

Fracture mechanism. The evolution of compressive stress as a function of strain of all specimens in group A is presented in Figure 15. It can be seen that similar

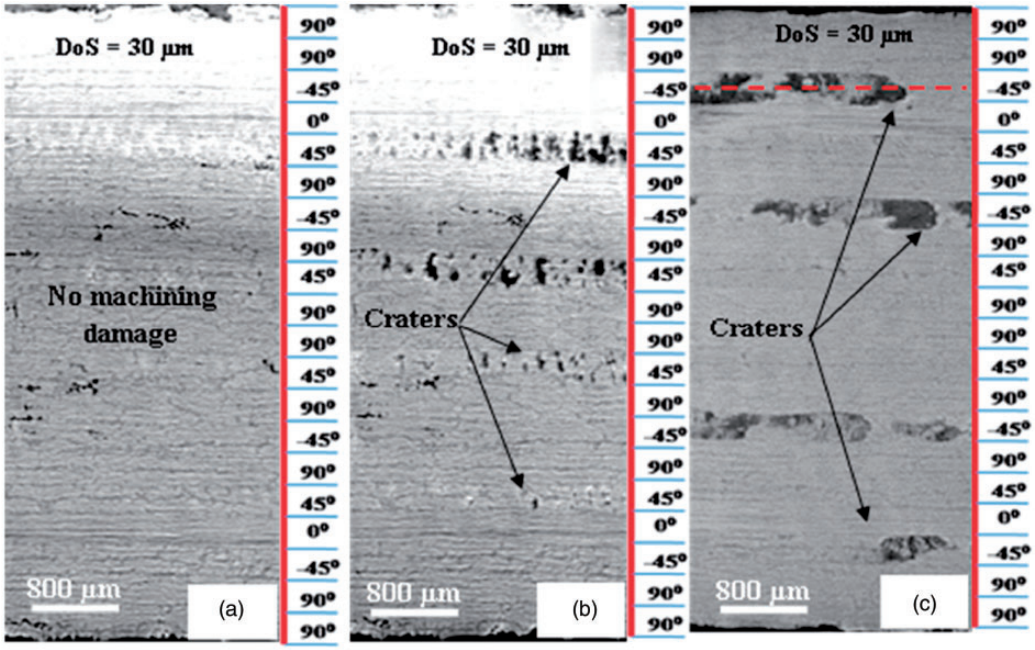

Figure 12. X-ray tomography images showing machining damage under machined surface of specimens in group A at depth of scanning of 30 μm with various cutting parameters (a) good quality with $V_c = 150$ m/min, $V_f = 500$ mm/min, and $L_c = 0.28$ m, (b) medium quality with $V_c = 150$ m/min, $V_f = 1500$ mm/min, and $L_c = 1.68$ m, and (c) poor quality with $V_c = 339$ m/min, $V_f = 29$ mm/min, and $L_c = 0.28$ m.

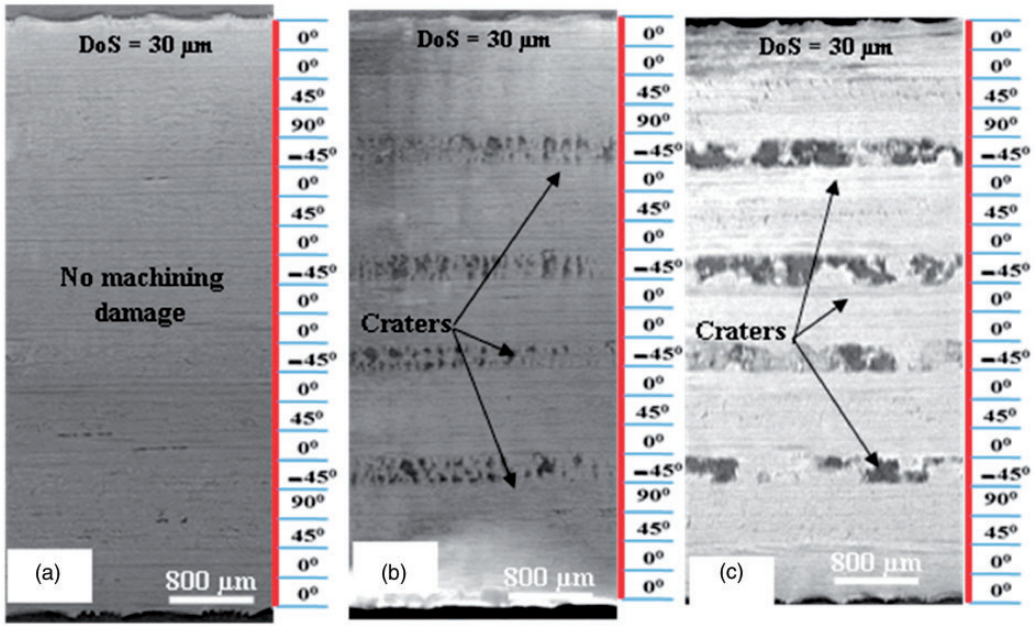

Figure 13. X-ray tomography images showing machining damage under machined surface of specimens in group B at depth of scanning of 30 μm with various cutting parameters (a) good quality with $V_c = 150$ m/min, $V_f = 500$ mm/min, and $L_c = 0.28$ m, (b) medium quality with $V_c = 150$ m/min, $V_f = 1500$ mm/min, $L_c = 1.68$ m, and (c) poor quality with $V_c = 339$ m/min, $V_f = 29$ mm/min, and $L_c = 0.28$ m.

behaviors of failure scenario were observed for other tested specimens in this group. However, the values of compressive strength, as well as failure strain of tested specimens are different. To better understand the failure scenario, the stress–strain curve of a specimen which is considered as poor surface quality with crater volume of $0.117\,mm^3/cm^2$ is selected to be representative for all specimens.

It is observed that failure scenario can follow four steps (Figure 16):

- Step 1: The stress increases linearly up to a strain of 0.0035. This increase then becomes non-linear until the first break. It can be seen that the first damage is characterized by the appearance of a crack or delamination at the –45°/0° interface corresponding to the third and fourth layer of the laminate when the load reaches 220 MPa (point a in the Figure 16).
- Step 2: After that a propagation of crack is observed, and the propagation is accompanied with buckling of the right side of the specimen, then the 0° ply breaks (fiber failure) at the maximum load of 270 MPa (point b in the Figure 16). We can also refer to the layers shown in Figure 12 where the –45°/0° interface is the first one to delaminate during compression, and 0° layer is the first ply to break during compression, and which are clearly damaged during the machining process.
- Step 3: An abrupt reduction of load up to 210 MPa is noted corresponding to the delamination of the –45°/0° interface at the left side and to the compressive fiber failure of the 0° ply (point c in the Figure 16).
- Step 4: Finally, a slight increase in the load up to 215 MPa is observed corresponding to appearance of total fracture (point d in the Figure 16).

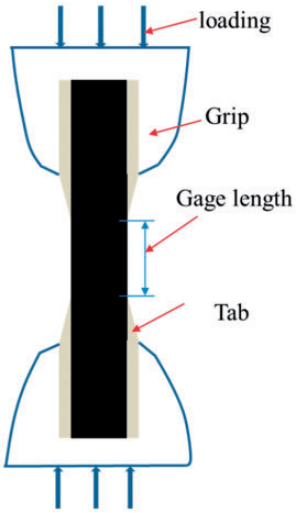

Figure 14. Schema of the compression test.

The appearance of the first crack is schematically shown in Figure 17. The sum up of failure process can be seen in the Figure 18 where the steps 1, 2, 3, and 4 are shown by images in the Figure 18(a), (b), (c), and (d), respectively. The first crack/delamination appearing during compressive loading are similarly observed of all tested specimens in this group could be the truth that the machining induces more matrix damage than fiber damage in this stacking sequence of group A. Furthermore, it is realized that the fracture mechanism in this study is similar to the one observed by Haddad et al.,[32] when the stacking sequences of two studies are similar.

A difference between the linear parts of the stress–strain curve obtained by experiment and by a

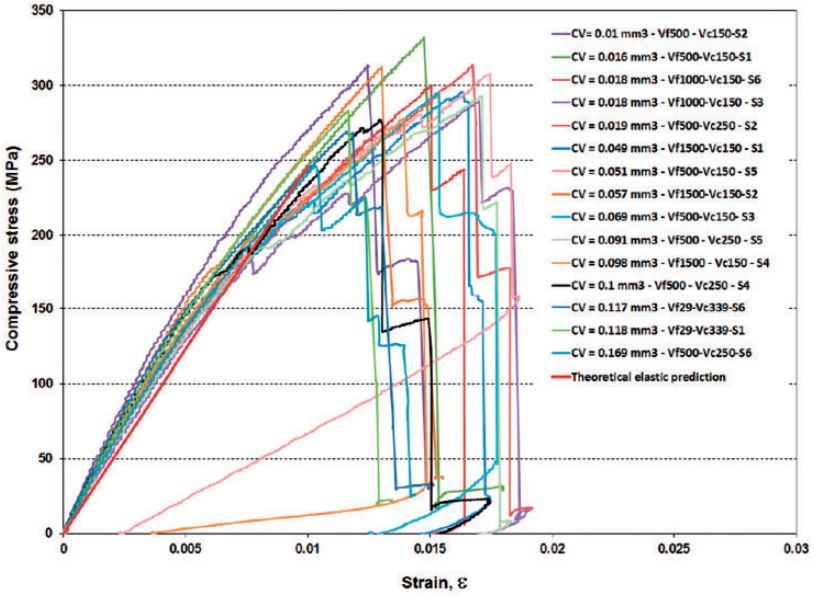

Figure 15. Evolution of compressive stress versus strain for specimens in group A.

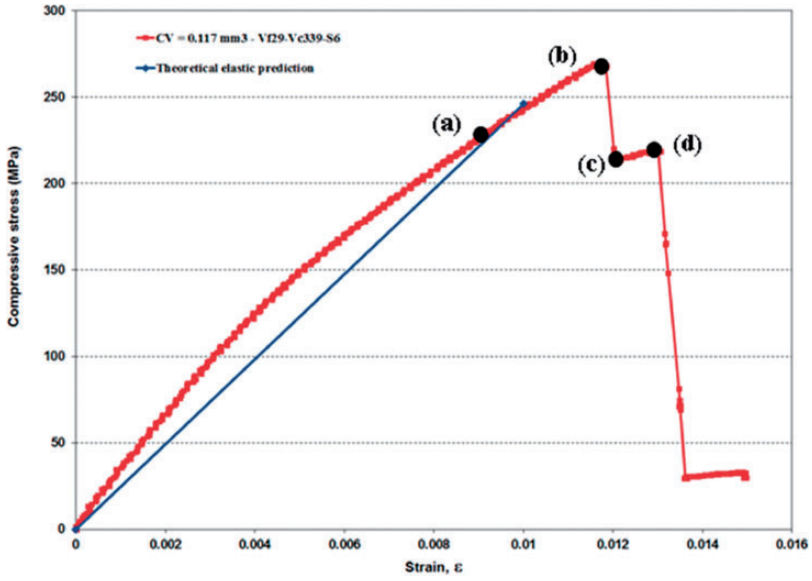

Figure 16. Evolution of the load vs displacement obtained for a representative specimen in group A.

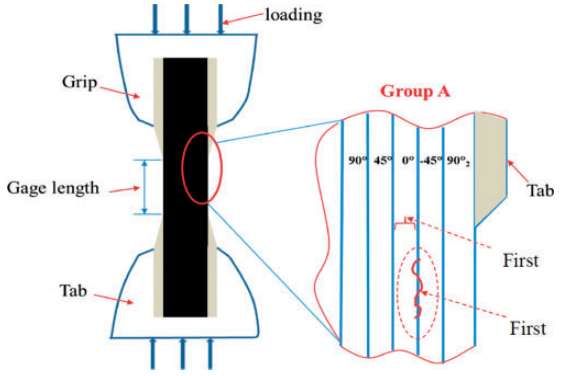

Figure 17. Schematic diagram showing the failure scenario of group A.

theoretical elastic prediction can be noticed (Figure 16). This elastic prediction was done using the classical laminate theory and the material characteristic given in Table 1. The objective of this prediction was to better understand the experimental test and in particular to evaluate a theoretical compressive failure stress of the pristine sample; this point will be discussed in the next section ''The influence of machining damage on the compressive strengths''. This difference between the experimental and the theoretical stiffness (Figure 16) should be partially due to the fact that the strain is evaluated with a linear extrapolation of the displacement measured by the machine, and the extrapolation coefficient is evaluated using the extensometer data and the test beginning. Then the strain measurement should be taken with caution. Of course, the best would have been to use extensometer in the gage part of the sample, but this part is too short to avoid the buckling of the sample. Moreover, it is not possible to use the extensometer until the end of the test, in order to avoid its damage.

Regarding the evolution of compressive strength versus strain resulting from the tests of specimens of group B, it is noticed that almost all specimens in group B have similar fracture mechanism as that present in Figure 19. Moreover, it is realized that the failure scenario in this group is different from that in group A when only two steps are observed during compressive loading, i.e. appearance of first crack and final failure of specimens. For the first step, based on the films obtained by infrared camera we realize that the first crack/delamination occurs randomly. It is not always in the same location in the stacking sequence for all tested specimens, and varying between layers upward two 0° layers; it can be located in the 0°/45° interface (the second and third layer), 45°/90° interface (the third and fourth layer), 90°/–45° interface (the fourth and fifth layer), or 0°/45° interface (the fifth and sixth layer). This is schematically described in Figure 20. For the final break, it occurs at the end zone of the tightening of the grips which is also a zone of important shear stress.

One more time it can be noticed a difference between the linear parts of the stress–strain curve obtained by experiment and by a theoretical elastic prediction (Figure 19). As previously mentioned this difference should be partially due to the strain evaluation using a linear extrapolation of the displacement measured by the machine and by the extensometer data; then the strain measurement should be once again taken with caution.

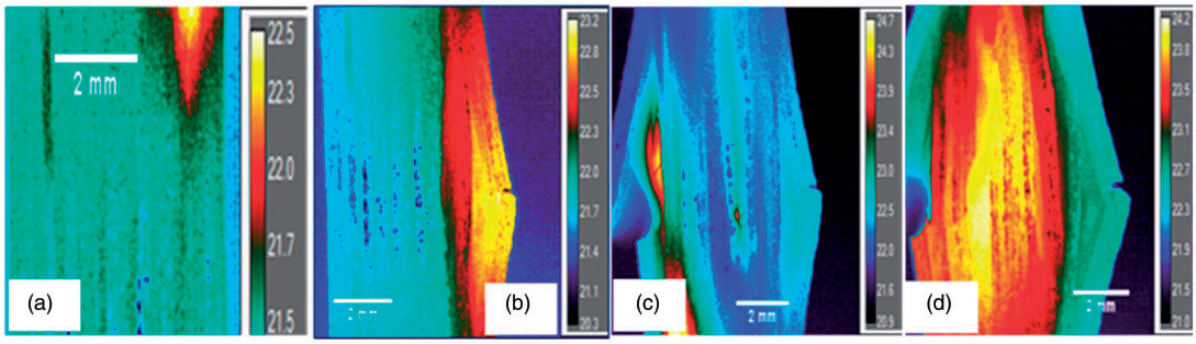

Figure 18. Images obtained by the infrared camera during compressive loading on a tested specimen of group A (a) appearance of the first crack, (b) propagation of the first crack/break (c) appearance of second break, and (d) final break.

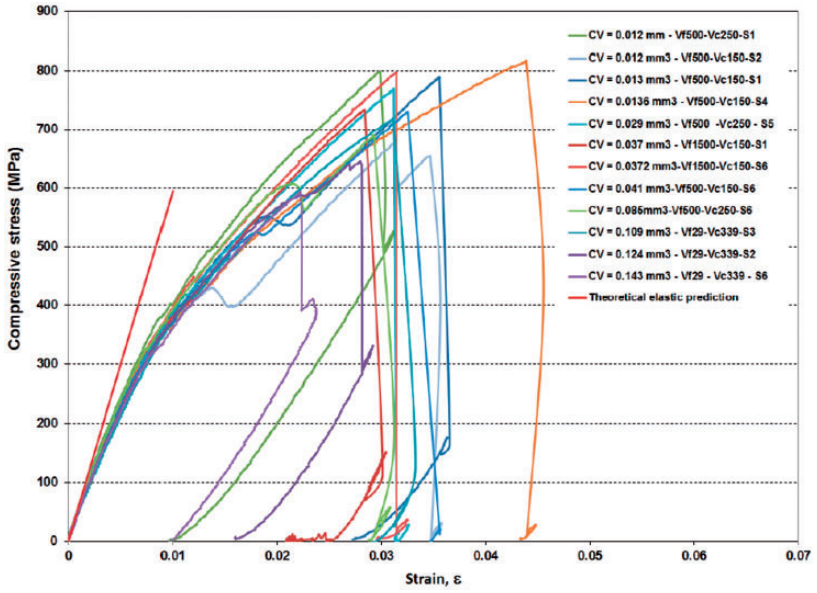

Figure 19. Evolution of compressive stress versus strain for specimens in group B.

To better understand the failure scenario of this group, a stress–strain curve of a specimen, which is considered as good surface quality with crater volume of 0.0147 mm^3/cm^2, is chosen to be the representative of all specimens in group B (Figure 21).

The failure scenario of specimens in group B can be observed with two steps:

- Step 1: It is observed that the stress increases linearly up to a strain of 0.0025 and then becomes non-linear till final break. The non-linearity, which is more pronounced than in the previous case, should be due to the more important sliding in the grips. Indeed the failure stress being higher than for the group A, the grips tightening was a little bit low and some additional displacement could be due to the sliding of the samples. To avoid this sliding, the ends of the samples were put on the grips ends. Moreover, the non-linearity is more or less pronounced depending on the tests (Figure 19). Then first crack/break (point a of the Figure 21), which is schematically presented in Figure 20, occurs in the 90°/–45° interface of the two layers corresponding to fourth and fifth layers in stacking sequence, when stress reaches value of 540 MPa (Figure 22(a)).
- Step 2: This crack propagates till the appearance of final break at maximum stress of 790 MPa (point b of the Figure 20). The final break occurs at the end zone of the tightening of the grips which is also a zone of important shear stress (Figure 22(b)).

The random occurrences of first delamination can be due to the fact that two layers of 0° (outermost layer) have strong ability to withstand in the loading

direction. Hence, these layers withstand others neighboring plies which are weak in loading direction. It means that the delamination appears before occurrence of the final compressive fiber failure, and its propagation is blocked by the outermost 0° layers. This hypothesis is based on the observations of the infrared films around the 0° layers (Figure 22(a)). In the previous case (group A), the delamination induced quickly the final break because the outermost layers were only unoriented layers with loading direction (90° and –45° layers). However, to better understand the failure scenario of this specimen group, more experiments should be done. Moreover, a finite element model simulation of this test could be considered as a better solution.

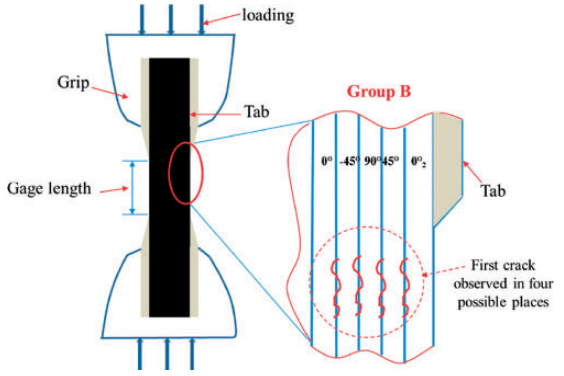

Figure 20. Schematic diagram showing the failure scenario of group B.

In the next section of this study, the relationships between machining damage and compressive strength will be discussed.

The influence of machining damage on the compressive strengths. To find the relationship between machining quality and mechanical behavior which has given a lot of ambiguities in literature as early described, compression tests were carried out on the trimmed specimens in groups A and B. Figure 23 presents the evolution of compressive strength of specimens in

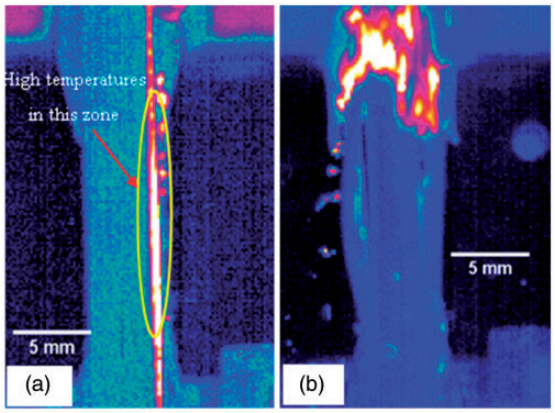

Figure 22. Images obtained by the infrared camera during compressive loading on a tested specimen of group B (a) appearance of the first crack in 90°/–45° interface (the fourth and fifth layer) and (b) final break.

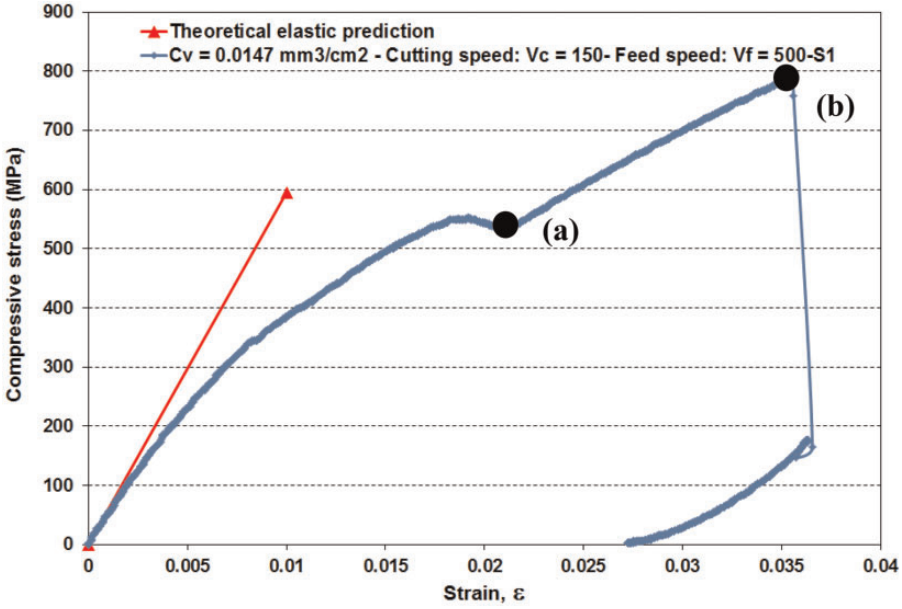

Figure 21. Evolution of the load vs displacement obtained for a representative specimen in group B.

group A as a function of machining quality which was characterized using surface roughness and crater volume. It is seen that an increase in surface roughness or crater volume leads to reduce compressive strength. However, it is difficult to correlate the relation between surface roughness and compressive strength due to huge scatter of results (Figure 23(a)). This is proved by low R-square value which is 0.4081. Inversely, crater volume seems to be a better indicator to correlate machining damage and compressive strength when R-squared value is as high as 0.8877 (Figure 23(b)). In this case, compressive strength totally decreases by approximately 22%, when crater volume increases from 0.01 mm^3/cm^2 to 0.169 mm^3/cm^2. The fact is that specimens with good quality have small damage levels which have less influence on the load carrying capacity of the specimens (Figure 10(a)). On the contrary, specimens with poor quality provide full of matrix degradation covering in the machined surfaces, moreover subsurface damage is superior to that of specimens with good and medium quality (Figure 10(c)). These factors induce discontinuity of the stress state and induce delamination, thus, reducing load carrying ability and compressive strength of specimens.

Regarding the correlation between surface quality and compressive strength in group B, the identical behaviors are also observed (Figure 24). It means that an increase in surface roughness or crater volume reduces the compressive strength, and the relations between crater volume and compressive strength

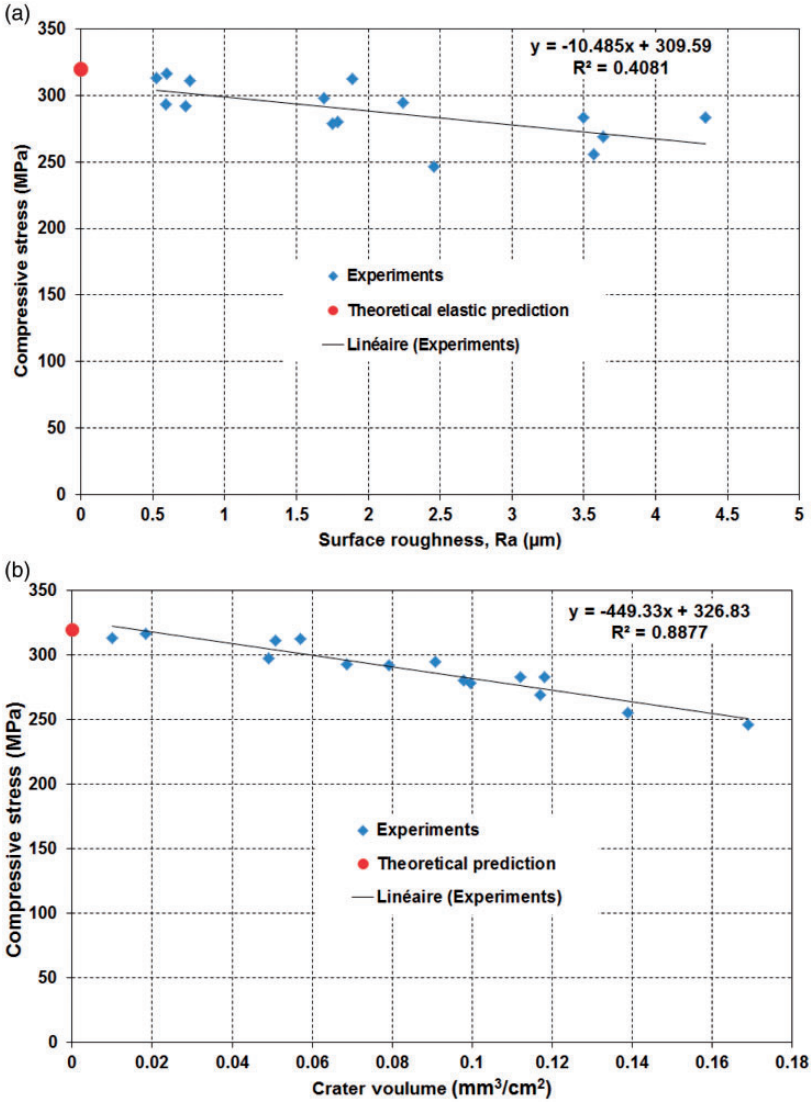

Figure 23. Evolution of compressive strength as a function of (a) surface roughness and (b) crater volume for tested specimens in group A.

(R-squared of 0.666) are more realistic than that between surface roughness and compressive strength (R-squared of 0.375). Moreover, it is noticed that the correlation between crater volume and compressive strength of specimens in group A is more consistent than that of specimens in group B. This can be due to the difference in stacking sequence of each type specimen which causes some unavoidable phenomena during the static test. Indeed, in case of group B, after testing of two first specimens we realized that slippage between specimens and tabs occurs (with detachment of the tabs). For this reason, the loading application in two sides of tabs and in the end of specimens for specimens in this group was performed. Some deformations of specimens, as well as small slippage might appear which could reduce the correlation between crater volume and compressive strength in this group as previously mentioned. Additionally, for the main part, the failure of group A is due to delamination of 0/–45 interface, and we observed the –45° ply is strongly damaged during machining (Figure 12). Then the poor machining should more degrade this interface strength. For the group B, the final failure is mainly due to the global failure of the 0° plies, and we observed that the machining damage has little effect on the 0° plies.

To evaluate the effect of machining compared to pristine samples, the values of compressive strength based on prediction in both group A and B was evaluated. The theoretical prediction value of compressive strength is evaluated based on the classical laminate theory, considering the failure of the first ply with

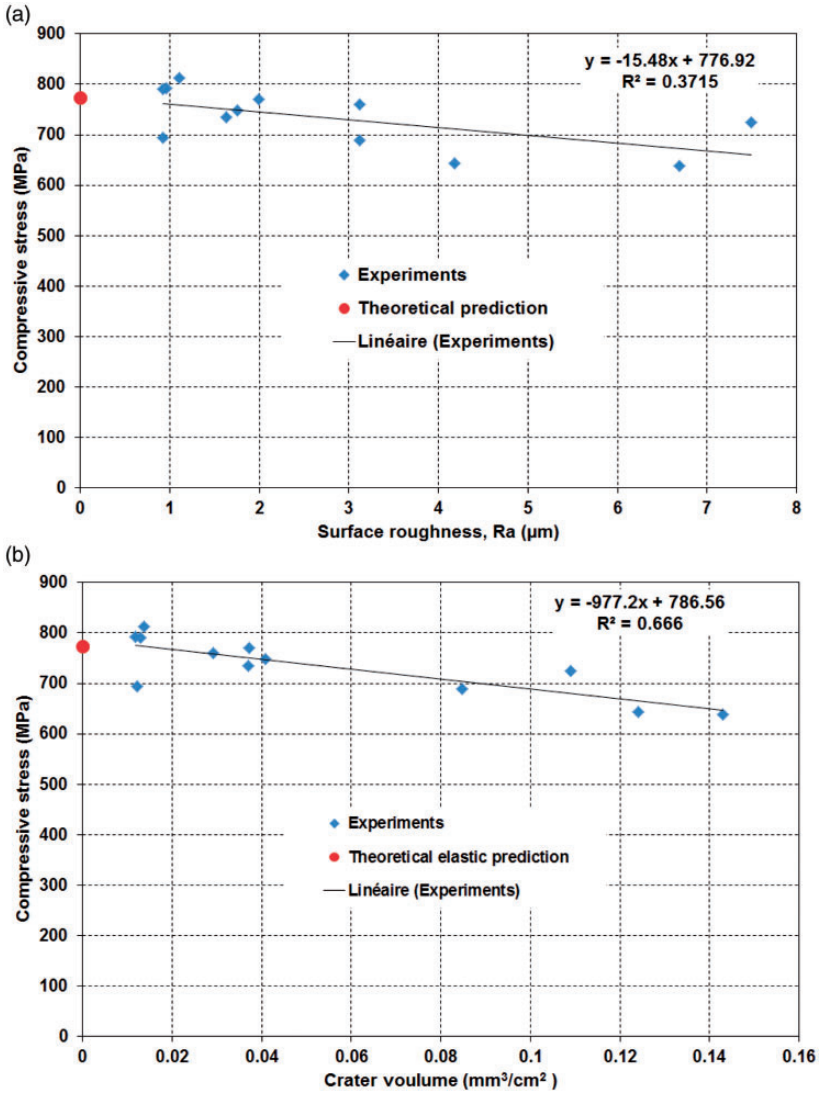

Figure 24. Evolution of compressive strength as a function of (a) surface roughness and (b) crater volume for tested specimens in group B.

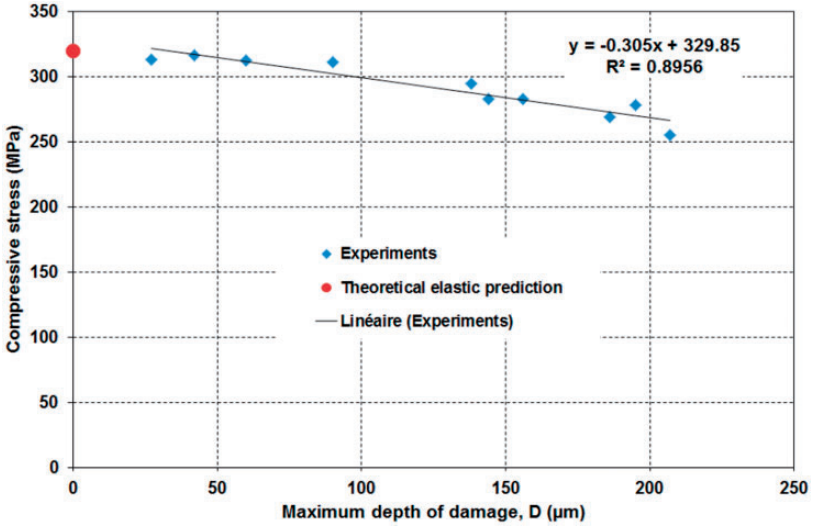

Figure 25. Evolution of compressive strength as a function of maximum depth of damage for tested specimens in group A.

a failure criterion of minimum compressive fiber strain as equation (1)

$$\varepsilon_{compression}^{fiber} = -0.013 \quad (1)$$

This value is compared to compressive strength obtained from experiments in order to evaluate the decrease of residual strength due to the machining. It is noticed that the predicted compressive strength is always higher than those gotten from experiments. This also reveals that when specimens possess good surface quality (small value of crater volume), the difference of compressive strength between prediction and experiment is logically small. Inversely, when specimens are characterized by poor quality (high value of crater volume) the difference of compressive strength is logically important.

To correlate maximum depth of machining damage (depth of craters), 10 tested specimens in group A were selected to X-ray tomography investigation. Figure 25 presents the evolution of compressive strength as a function of maximum depth of damage (D). Based on this figure, it can be observed that the correlation between maximum depth of damage and compressive strength is very good; indeed the R-squared value reaches almost 0.9. This result is realistic and logical because the holes/craters generated during machining are quantified in terms of depth where stress concentration factor plays an important role to reduce loading ability of composite structures during services.

Conclusions

This study focuses on the influence of the machining-induced damage on the mechanical behavior of the trimmed specimens during quasi static compressive tests. These tests have been conducted on transverse and longitudinal direction of the principal orientation of the multi-directional CFRP specimens. The machined surface was subjected to multi-scale characterization using SEM, X-ray tomography, and 3D profilometer.

Fracture mechanism of specimens in groups A and B in compressive loading is initiated by delamination, and the final fracture is due to compressive fiber failure. It seems the machining quality involves the delamination with the logical link: worse is the machining, higher is the roughness, higher is the interface damage and earlier is the delamination propagation; then lower is the residual strength.

The adverse effect of the machining damage on the compressive strength in group A is more significant than those of group B. Indeed, this can be explained by the fact that, the machining induces more matrix damage than fiber damage, and therefore, group A (which is matrix dominated) is more affected by machining damage than group B which is fiber dominated.

Finally, based on the multi-scale characterization of the machining damage, new surface quality criteria namely crater volume (C_v) and depth of damage (D) are proposed and correlated to mechanical behavior under compressive loading. These two new surface quality criteria seem to be good indicators to quantify machining quality of composite to better correlate with the mechanical behavior compared to the surface roughness criteria.

Declaration of Conflicting Interests

The author(s) declared no potential conflicts of interest with respect to the research, authorship, and/or publication of this article.

Funding

The author(s) received no financial support for the research, authorship, and/or publication of this article.

ORCID iD

C Bouvet https://orcid.org/0000-0003-2637-9170

References

1. Sheikh-Ahmad JY. *Machining of polymer composites*. Berlin: Springer, 2009.
2. Haddad M, Zitoune R, Eyma F, et al. Machinability and surface quality during high speed trimming of multi directional CFRP. *Int J Mach Mach Mater* 2013; 13: 289–310.
3. Slamani M, Chatelain J-F and Hamedanianpour H. Influence of machining parameters on surface quality during high speed edge trimming of carbon fiber reinforced polymers. *Int J Mater Form* 2019; 12: 331–353.
4. Hejjaji A, Singh D, Kubher S, et al. Machining damage in FRPs: laser versus conventional drilling. *Compos Part A – Appl Sci Manuf* 2016; 82: 42–52.
5. Hejjaji A, Zitoune R, Crouzeix L, et al. Surface and machining induced damage characterization of abrasive water jet milled carbon/epoxy composite specimens and their impact on tensile behavior. *Wear* 2017; 376–377: 1356–1364.
6. Nguyen-Dinh N, Hejjaji A, Zitoune R, et al. Machining of FRP composites: surface quality, damage, and material integrity: critical review and analysis. In: Sarabjeet SS, Preetkanwal SB, Redouane Z and Morteza Y (eds) *Futuristic composites*. Berlin, Germany: Springer, 2018, chapter 1, pp.1–35.
7. Koplev A, Lystrup A and Vorm T. The cutting process, chips, and cutting forces in machining CFRP. *Composites* 1983; 14: 371–376.
8. Wangf DH, Ramulu M and Arola D. Orthogonal cutting mechanisms of graphite/epoxy composite – part II: multidirectional laminate. *Int J Mach Tools Manuf* 1995; 35: 1639–1648.
9. Wang DH, Ramulu M and Arola D. Orthogonal cutting mechanisms of graphite/epoxy composite. Part I: unidirectional laminate. *Int J Mach Tools Manuf* 1995; 35: 1623–1638.
10. Zitoune R, Collombet F, Lachaud F, et al. Experiment–calculation comparison of the cutting conditions representative of the long fiber composite drilling phase. *Compos Sci Technol* 2005; 65: 455–466.
11. Colligan K and Ramulu M. Delamination in surface plies of graphite/epoxy caused by edge trimming process. *Process Manuf Compos Mater* 1991; 113–125.
12. Hintze W, Hartmann D and Schütte C. Occurrence and propagation of delamination during the machining of carbon fibre reinforced plastics (CFRPs) – an experimental study. *Compos Sci Technol* 2011; 71: 1719–1726.
13. Sheikh-Ahmad J, Urban N and Cheraghi H. Machining damage in edge trimming of CFRP. *Mater Manuf Process* 2012; 7: 802–808.
14. Sheikh-Ahmad J and Shahid AH. Effect of edge trimming on failure stress of carbon fibre polymer composites. *Int J Mach Mach Mater* 2013; 13: 331–347.
15. Duboust N, Melis D, Pinna C, et al. Machining of carbon fibre: optical surface damage characterisation and tool wear study. *Procedia CIRP* 2016; 45: 71–74.
16. Prakash R, Krishnaraj V, Zitoune R, et al. High-speed edge trimming of CFRP and online monitoring of performance of router tools using acoustic emission. *Materials* 2016; 9: 798–808.
17. Haddad M, Zitoune R, Eyma F, et al. Study of the surface defects and dust generated during trimming of CFRP: influence of tool geometry, machining parameters and cutting speed range. *Compos Part A* 2014; 66: 142–154.
18. Silva P, Ferreira F, Abreu SM, et al. Correlation of drilling damage with mechanical strength. *Comp Struct* 2017; 181: 306–314.
19. Silva P, Matos JE and Durão LMP. Analysis of damage outcome in the strength of polymer composite materials. *J Comp Mat* 2019; 53: 547–560.
20. Wang F, Yin J, Jia Z, et al. A novel approach to evaluate the delamination extent after edge trimming of carbon-fiber-reinforced composites. *Proc Inst Mech Eng, Part B: J Eng Manuf* 2017; 232: 2523–2532.
21. Wang F, Yin J, Ma J, et al. Effects of cutting edge radius and fiber cutting angle on the cutting-induced surface damage in machining of unidirectional CFRP composite laminates. *Int J Adv Manuf Technol* 2017; 91: 3107–3120.
22. Hejjaji A, Zitoune R, Toubal L, et al. Influence of controlled depth abrasive water jet milling on the fatigue behavior of carbon/epoxy composites. *Compos Part A: Appl Sci Manuf* 2019; 121: 397–410.
23. Davim JP, Reis P and António CC. A study on milling of glass fiber reinforced plastics manufactured by hand-lay up using statistical analysis (ANOVA). *Compos Struct* 2004; 64: 493–500.
24. Kim D, Kim YH, Gururaja S, et al. Processing and fiber content effects on the machinability of compression moulded random direction short GFRP composites. *Int J Automot Technol* 2010; 11: 849–855.
25. Janardhan P, Sheikh-Ahmad J and Cheraghi H. Edge trimming of CFRP with diamond interlocking tools, SAE Tech Papers, 2006, 2006-01-3173.
26. Nguyen-Dinh N, Zitoune R, Bouvet C, et al. Surface integrity while trimming of composite structures: X-ray tomography analysis. *Compos Struct* 2019; 210: 735–746.
27. Cadorin N, Zitoune R, Seitier P, et al. Analysis of damage mechanism and tool wear while drilling of 3D woven composite materials using internal and external cutting fluid. *J Compos Mater* 2015; 49: 2687–2703.
28. Arola D and Ramula M. Machining-induced surface texture effects on the flexural properties of a graphite/epoxy laminate. *Composites* 1994; 25: 822–834.
29. Ghidossi P, Mansori ME and Pierron F. Influence of specimen preparation by machining on the failure of polymer matrix off-axis tensile coupons. *Compos Sci Technol* 2006; 66: 1857–1872.

30. Eriksen E. The influence of surface roughness on the mechanical strength properties of machined short-fibre-reinforced thermoplastics. *Compos Sci Technol* 2000; 60: 107–113.
31. Squires CA, Netting KH and Chambers AR. Understanding the factors affecting the compressive testing of unidirectional carbon fibre composites. *Compos Part B: Eng* 2007; 38: 481–487.
32. Haddad M, Zitoune R, Eyma F, et al. Influence of machining process and machining induced surface roughness on mechanical properties of continuous fiber composites. *Exp Mech* 2015; 55: 519–528.
33. Ramulu M. Characterization of surface quality in machining of composites. *Manuf Eng Mater Process* 1999; 53: 575–648.
34. Zitoune R, Cadorin N, Collombet F, et al. Temperature and wear analysis in function of the cutting tool coating when drilling of composite structure: in situ measurement by optical fiber. *Wear* 2017; 376: 1849–1858.
35. Haddad M, Zitoune R, Bougherara H, et al. Study of trimming damages of CFRP structures in function of the machining processes and their impact on the mechanical behavior. *Compos Part B: Eng* 2014; 57: 136–143.